Disposable electrochemical detection of breast cancer tumour marker CA 15-3 using poly(Toluidine Blue) as imprinted polymer receptor

J.A. Ribeiro, C.M. Pereira, A.F. Silva, M.Goreti F. Sales

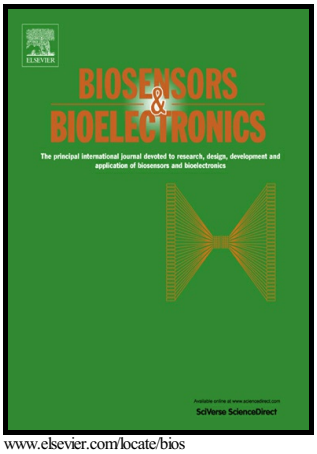

www.elsevier.com/locate/bios

PII: S0956-5663(18)30174-X
DOI: https://doi.org/10.1016/j.bios.2018.03.011
Reference: BIOS10337

To appear in: *Biosensors and Bioelectronic*

Received date: 8 November 2017
Revised date: 28 February 2018
Accepted date: 6 March 2018

Cite this article as: J.A. Ribeiro, C.M. Pereira, A.F. Silva and M.Goreti F. Sales, Disposable electrochemical detection of breast cancer tumour marker CA 15-3 using poly(Toluidine Blue) as imprinted polymer receptor, *Biosensors and Bioelectronic,* https://doi.org/10.1016/j.bios.2018.03.011

Disposable electrochemical detection of breast cancer tumour marker CA 15-3 using poly(Toluidine Blue) as imprinted polymer receptor

J.A. Ribeiro[a,b*], C.M. Pereira[a*], A. F. Silva[a], M. Goreti F. Sales[b]

[a] *CIQUP/Department of Chemistry and Biochemistry, Faculty of Sciences, University of Porto, Portugal*

[b] *BioMark/CINTESIS-ISEP, School of Engineering, Polytechnic Institute of Porto, Portugal*

***Corresponding Author:** E-mail addresses: cmpereir@fc.up.pt (C.M. Pereira), jadribeiro@gmail.com (J.A. Ribeiro).

Abstract

In this work, electrically-conducting poly(Toludine Blue) was employed for the first time as synthetic receptor film, prepared by Molecular Imprinting strategies and using electrochemical methods, for the specific screening of breast cancer biomarker Carbohydrate Antigen 15-3 (CA 15-3).

The protein imprinted poly(Toluidine Blue) film was grown in a pre-formed Toluidine Blue (TB) tailed SAM at the AuSPE surface, which greatly enhanced the stability against degradation of the Molecular Imprinted Polymer (MIP) film at the electrode surface.

The MIP receptor film recognition ability towards the protein was investigated by fitting data to Freundlich isotherm. The binding affinity (K_F) obtained for the MIP system was significantly higher

(~12-fold) to that obtained for the NIP system, demonstrating the success of the approach in creating imprinted materials that specifically respond to CA 15-3 protein.

The incubation of the MIP modified electrode with increasing concentration of protein (from 0.10 U mL^{-1} to 1000 U mL^{-1}) resulted in a decrease of the ferro/ferricyanide redox current. The device displayed linear response from 0.10 U mL^{-1} to 100 U mL^{-1} and LODs below 0.10 U mL^{-1} were obtained from calibration curves built in neutral buffer and diluted artificial serum, using DPV technique, enabling the detection of the protein biomarker at clinically relevant levels. The developed MIP biosensor was applied to the determination of CA 15-3 in spiked serum samples with satisfactory results.

The developed device provides a new strategy for sensitive, rapid, simple and cost-effective screening of CA 15-3 biomarker. Importantly, the overall approach seems suitable for point-of-care (PoC) use in clinical context.

Keywords: Biosensor; Carbohydrate Antigen 15-3; Toluidine Blue; Screen-printed gold electrode; Molecularly-imprinted polymer.

1. Introduction

Breast cancer is by far the most commonly diagnosed cancer and the leading cause of cancer death in women worldwide, with an estimated 1.7 million diagnosed new cases and 521,900 deaths, in 2012 (Jemal et al. 2010).

Biomarkers currently play a key role in the management of patients with breast cancer, especially in follow-up of the disease (Jin et al. 2017; Sturgeon et al. 2008). In this context, Carbohydrate Antigen 15-3 (CA 15-3), a mucin-like glycoprotein (≈ 400 kDa) secreted by breast cancer cells, is the most widely used serum marker for breast cancer (Chourin et al. 2009; Duffy et al. 2004; Sölétormos et al. 2004). Its main applications include the surveillance of patients following surgery, deciding whether to persist in using a particular type of therapy, terminate its use, or switch to an alternative therapy. For healthy humans, the levels of CA15-3 are lower than 30 U mL^{-1}, while patients with high postsurgical concentrations (>30 U mL^{-1}) have shorter overall survival pattern than those with low concentrations levels (Chourin et al. 2009; Duffy et al. 2004; Sölétormos et al. 2004).

Most of the methods reported for detecting CA 15-3 rely on immunoassays with different signal transduction approaches, such as ELISA (Ambrosi et al. 2010; Gonzalez et al. 2008), SPR (Chang et al. 2010), Optofluidic Ring Resonator (Zhu et al. 2009), flow-based fluorescence (Darwish et al. 2012; Park et al. 2013), chemiluminescence (Fu et al. 2007; Zong et al. 2012) electrochemiluminescence (Jiang et al. 2015), SECM (Zhang et al. 2006), SERS (Li et al. 2015) and electrochemical (Akter et al. 2016; Fragoso et al. 2011; Ge et al. 2012a; Ge et al. 2012b; Li et al. 2013; Li et al. 2010; Liu et al. 2011; Wang et al. 2013; Wu et al. 2015b). Although these biosensors are very selective due to the use of biological recognition molecules that are highly specific for a target analyte they usually have the disadvantages of being technically complicated (loss of antibody activity), time-consuming and rather expensive (Whitcombe et al. 2011). Thus, there is a steadily

growing interest in mimicking natural recognition systems using synthetic analogs aiming to overcome some limitations related to immunosensors.

Recently, molecularly imprinted polymers (MIPs) have been extensively used by researchers to create biomimetic materials with easy integration into transducers to develop novel formats for electrochemical sensors (Malitesta et al. 2012; Sharma et al. 2012) able to recognize and respond to (bio)molecules of interest, such as proteins (Erdőssy et al. 2016; Gui et al. 2018; Kryscio and Peppas 2012; Moreira et al. 2014; Rebelo et al. 2014; Ribeiro et al. 2017; Whitcombe et al. 2011). Moreover, the rigid nature of the polymer may lead to long-term storage stability, robustness and potential re-usability of devices (Whitcombe et al. 2011; Ye and Mosbach 2008).

Among the most commonly used MIP preparation procedures, such as drop-coating, composite making or spin-coating, etc., MIP films prepared by electrochemical polymerization have unique advantages (Erdőssy et al. 2016; Malitesta et al. 2012; Sharma et al. 2012), such as (1) simple and fast preparation, (2) high adherence to the electrode surface, (3) easy control of the film thickness and morphology and (4) high reproducibility in different conductive materials. Once polymerization is complete, the template molecule is subsequently extracted from the polymeric matrix using a suitable approach leaving specific recognition sites available for (re)binding.

Phenazines have not been previously employed in the preparation of imprinted materials for proteins, despite their electrocatalytic features and subsequent ability to form polymers under electropolymerization. These poly(phenazine) redox polymers are conductive since they retain monomer type redox activity after polymerization, which makes them very attractive in electroanalysis (Cai and Xue 1998; Karyakin et al. 1999; Pauliukaite et al. 2010; Schlereth and Karyakin 1995).

Toluidine blue (TB, shown in Scheme S1, SI), a member of the water-soluble azine-type redox dye family, has unique chemical and electrochemical properties that lead to their extensive use as electronic mediator in the construction of enzymatic electrodes for biosensing applications (Moon et

al. 2017; Peng et al. 2015; Thenmozhi and Narayanan 2017; Wang et al. 2014a, b; Zhang and Gorski 2005). At a sufficiently high electrode potential, electropolymerization of the dye at electrode occurs surface (Lu et al. 2009; Mažeikienė et al. 2008) giving origin to effective 3D mediator structures with improved electrocatalytic activity, already tested in electroanalytical context towards some common redox bioactive compounds, such as NADH (Zhai et al. 2013), nitric oxide (Wang and Hu 2006), H_2O_2 (Chang et al. 2013; Lu et al. 2009) and glucose (Wang et al. 2010).

Although electropolymerization of phenazines can occur directly on bare electrode surfaces, sometimes, it is difficult to form polymer films with a good stability and space filling on metal surfaces due to the poor adhesion between the growing phase and the substrate, which inhibits the nucleation and the growth of film along the substrate. Alternatively, the polymer can be grown from well-organized self-assembled monolayers (Ju et al. 2002; Schlereth and Schmidt 1995), improving the adhesion of the polymer film to the electrode surface (see Scheme 1).

The novelty of this work arises from the use of TB for the first time as the monomer to fabricate an electrically conductive MIP based electrochemical sensor for detection of CA 15-3. The fabrication of the disposable biosensing device is technically simple and the time and cost of the analysis considerably reduced when compared to the previously reported immunoassays used for CA 15-3 detection, offering the possibility of biomarker screening in PoC with good sensitivity and selectivity. In this work, the electroactive poly(TB) film was tethered to the AuSPE surface *via* Au–S bonds due to the cross-linking between TB tailed monolayer and the TB monomer in solution by electrochemical polymerization (see Scheme 1) which greatly enhances the stability of the polymer film at the Au substrate.

Scheme 1

2. Experimental section

2.1. Chemicals and solutions

Carbohydrate Antigen 15-3 (CA 15-3) MUC 1 Antigen (24 kU mL^{-1}, EastCoast Bio), Toluidine Blue (Merck, Darmstadt), 8-amino-1-octanethiol (AOT, hydrochloride, Dojindo Laboratories), potassium ferricyanide ($K_3[Fe(CN)_6]$, ≥ 99.0%, Fluka) and potassium ferrocyanide ($K_4[Fe(CN)_6].3H_2O$, p.a., ≥ 99.5%, Fluka) were used as received. Phosphate buffer solution (PBS) 0.1 mol L^{-1} (at pH 7.4) consisted of sodium dihydrogen phosphate dihydrate (p.a., Sigma-Aldrich) and anhydrous disodium hydrogen phosphate (p.a., Fluka). Standard stock solution of CA 15-3 6.7 kU mL^{-1} was prepared in PBS 0.1 mol L^{-1} (at pH 7.4) and stored at −20 °C if not in use. Less concentrated standards were obtained by accurate dilution of the previous solution, in the same buffer. $K_3[Fe(CN)_6]$)/$K_4[Fe(CN)_6]$ (1:1, 5 mmol L^{-1}) redox probe solution was prepared in 0.1 mol L^{-1} Na_2SO_4. Unless otherwise stated, all the other chemicals and reagents used were of analytical grade. All aqueous solutions were prepared using water purified with a Milli-Q purification system (resistivity ≥ 18 MΩ cm).

2.2. Apparatus

Electrochemical data were obtained using a computer-controlled potentiostat Autolab PGSTAT30 (Eco Chemie B.V., Utrecht, Netherlands) monitored by the NOVA 1.11 software package.

Gold screen-printed electrodes (AuSPEs) were purchased from DropSens (DRP-220AT). They include a gold disk-shaped (12.6 mm^2) working electrode, a silver pseudo-reference electrode and a gold counter electrode, all of them screen-printed on a ceramic substrate (3.3 cm×1.0 cm) and subjected to high-temperature curing. All potential values were referred to the screen-printed silver

pseudo-reference electrode. The SPEs were connected to a switch box, also from DropSens (DRP-DSC), allowing their interface with the potentiostat. All experiments were carried out at room temperature (21 °C).

Raman spectrometry with confocal microscopy measurements were performed using a Thermo Scientific DXR Raman microscope equipped with a 785 nm laser, in combination with a 50× objective magnification for focusing and collection of Raman-scattered light. An incident maximum laser power of 1 mW was applied in order to avoid peak shifts due to thermal heating or structure transformations during data acquisition. Raman spectra were collected with a slit aperture of 50 μm.

2.3. Monolayer preparation

Prior to modification, the AuSPEs were washed thoroughly with ethanol and acetone followed by electrochemical cleaning by cycling the electrode potential from 0 to 1.05 V at a rate of 100 mV s^{-1} in 0.1 mol L^{-1} sulfuric acid until the CV becomes stable (approximately 12 cycles). Finally, the electrodes were washed with ultrapure water.

The AOT self-assembled monolayer was prepared by incubation of the working electrode with 18 mmol L^{-1} AOT aqueous solution (10 μL drop) overnight, at room temperature. The electrode was rinsed with water and dried under nitrogen flow. The amine-modified electrode was then imine-derived by incubating it with an aqueous solution of glutaraldehyde (12% v/v) for 1 hour. Then, the remaining aldehyde functional moieties at the SAM surface were allowed to react with the aromatic amino group of the phenothiazine by performing potential cyclic scans at 50 mV s^{-1} between -0.45 and 0.10 V in 0.1 mol L^{-1} PBS (at pH 7.4), containing 0.5 mmol L^{-1} of TB (45 μL drop) until a stable cyclic voltammogram was obtained (usually 10 sweep cycles). Then, the modified electrodes were cycled, usually 25 cycles, at 50 mV s^{-1}, over the same potential range in 0.1 mol L^{-1} PBS (at pH 7.4) to promote desorption of the physically adsorbed material.

2.4. Preparation of MIP receptor

Protein imprinted poly(TB) films were grown in TB tailed SAM by electropolymerizing 0.5 mmol L^{-1} TB in PBS 0.1 mol L^{-1} (at pH 7.4) in the presence of 6.7 kU mL^{-1} of CA 15-3. The thickness of the film depended on the number of cycles. Electropolymerization was conducted along 60 cyclic voltammograms between -0.50 and 0.70 V, at the scan rate of 20 mV s^{-1}. A similar procedure, excluding the presence of CA 15-3, was employed in the fabrication of control non-imprinted polymer (NIP) modified electrodes. Finally, the resulting modified electrode surface was cycled from -0.55 or -0.65 to 0.35 V, at 50 mV s^{-1}, in 0.1 mol L^{-1} PBS (at pH 7.4) containing 0.1 mol L^{-1} $NaNO_3$ (dopant), until a stable voltammogram was obtained, to remove physically adsorbed material, dried under a nitrogen flow and stored properly at room temperature for further use.

CA 15-3 was successfully washed out from the polymeric matrix after continuous potential cycling the electrode surface between 0.00 and 0.40 V at 50 mV s^{-1} in 0.1 mol L^{-1} NaOH for 200 cycles (≈1 hour repetitive scans), followed by subsequent extensive washing with ultrapure water.

For characterization of the polymerized films, before and after template removal, several electrochemical techniques (CV, SWV and EIS) in the presence of ferro/ferricyanide redox probe were used. Each of the following post-polymerization treatments were also performed on NIP electrodes as a control, to confirm the success of the extraction procedure tested without destroying the backbone of the polymer network or the TB monolayer supporting the polymer. Raman measurements were also performed at this point.

2.5. Electrochemical measurements

In order to characterize the imprinted electrodes, electrochemical measurements were carried out in the presence of 5 mmol L^{-1} $K_3[Fe(CN)_6]/K_4[Fe(CN)_6]$ (1:1) solution containing 0.1 mol L^{-1} Na_2SO_4. The modified surfaces were coated with a 45 µL drop of the redox probe solution.

Cyclic voltammetry (CV) was performed at a scan rate of 50 mV s^{-1} and differential pulse voltammetry (DPV) operated under the following conditions: step potential of 4 mV, pulse amplitude of 50 mV and scan rate of 8 mV s^{-1}. Voltammograms collected with the imprinted electrode were recorded in the potential range of -0.30 to 0.50 V.

Electrochemical Impedance Spectroscopy (EIS) measurements were performed using a frequency scan ranging from 10,000 to 0.01 Hz and a sine wave perturbation of 10 mV rms. 60 frequency values were collected at the formal potential of the $[Fe(CN)_6]^{3-/4-}$ redox couple. Experimental spectra were presented in the form of complex plane diagrams (i.e., Nyquist plots) and were fitted with proper equivalent circuits, using the NOVA 1.11 software.

Binding isotherm was fitted to experimental data by non-linear least squares regression analysis using Igor Pro 6.22A software.

2.6. Calibration curves and binding affinity of CA 15-3 MIP receptor

Calibration curves were built to monitor the sensor response to CA 15-3 after incubating the electrode surface for 30 min with the appropriate concentration of CA 15-3 (from 0.10 U mL^{-1} to 1000 U mL^{-1}, in 0.1 mol L^{-1} PBS at pH 7.4), followed by washing with water to remove any loosely bound materials that could have been absorbed at the surface. This solution was then replaced by a drop of the 5 mmol L^{-1} $[Fe(CN)_6]^{3-/4-}$ redox probe solution for the electrochemical measurements.

Calibration curves were obtained by DPV measurements. A control monitoring was also performed for the NIP receptor film.

The MIP biosensor prepared was also tested in practical analysis against artificial serum samples containing known concentrations of CA 15-3. The artificial serum solution contained (Sayıklı Şimşek et al. 2015): 4.5 mmol L^{-1} KCl (Fluka), 5.0 mmol L^{-1} $CaCl_2$ (≥ 97.0%, Fluka), 1.6 mmol L^{-1} $MgCl_2$ (p.a., Riedel-de Haen), 4.7 mmol L^{-1} D(+)-glucose (Merck), 2.5 mmol L^{-1} urea (puriss, Sigma-Aldrich), 0.1% bovine serum albumin (BSA, ≥ 96%, Sigma) and 145 mmol L^{-1} NaCl (suprapur, Merck).

CA 15-3 samples and standard solutions were prepared by dilution of serum 10 times in 0.1 mol L^{-1} PBS (at pH 7.4). CA 15-3 determination in synthetic serum samples was also performed by DPV measurements.

3. Results and Discussion

3.1. General considerations

Practical prospects for application of the conducting polymer were taking into account, by investigating the physical and electrochemical stability of the polymer under the operating conditions. Therefore, a TB terminated monolayer was attached to the AuSPE surface from which poly(TB) was grown, aiming to enhance the stability of the MIP receptor film at the electrode surface (Ju et al. 2002; Schlereth and Schmidt 1995). In addition, the experimental conditions (potential window, supporting electrolyte, pH, etc.) were carefully selected to avoid polymeric backbone degradation with a consequent loss of electrical conductivity (Pud 1994).

The stability of the poly(TB) at the AuSPE surface was examined by repetitive scans in the potential range of -0.65 to 0.35 V, at 50 mV s^{-1}, in 0.1 mol L^{-1} PBS (at pH 7.4) containing 0.1 mol L^{-1} $NaNO_3$.

No significant changes in height (< 10%) and separation of voltammetric peaks were observed after 100 consecutive scans, showing no appreciable loss of electroactivity in the course of cycling. The presence of $NaNO_3$ dopant molecules in the electolyte contributed to the charge neutralizion and polymer backbone stabilization (Balint et al. 2014).

3.2. TB terminated monolayer

It is well known that the amine-terminated thiols act as bifunctional building blocks. In these, the thiol group binds to the Au surface and the amino group remains exposed to the outer surface, which may be employed for the subsequent attachment of other functional groups (Arias et al. 1996; Jiang et al. 2003; Willner et al. 1996; Willner and Riklin 1994; Xiao et al. 1999). In the present study, a medium-alkane-chain-length amine thiol (AOT) was chosen to be self-assembled on the AuSPE surface. Then, the bifunctional reagent, glutaraldehyde, reacted with the amino tails of the SAM to create imine bonds. After that, the glutaraldehyde moieties covering the modified SAM were allowed to react with the aromatic amino group of the phenothiazine by covering the modified electrode with 0.5 mmol L^{-1} solution of TB in 0.1 mol L^{-1} PBS (at pH 7.4), and driving cyclic potential scans between -0.45 and 0.10 V, until a stable cyclic voltammogram was obtained (typically after 10 CV scans; see Fig. 1A). It is important to notice that during this process the potential window was carefully chosen to avoid oxidation of TB units at the electrode surface and prevent the formation of a polymerized monolayer.

After the covalent attachment of TB onto the SAM monolayer, two voltammetric peaks (I and II) were observed in CVs performed in 0.1 mol L^{-1} PBS (at pH 7.4) shown in Fig. 1B. The redox peak I (centred at -0.25 V), which retained the original redox potential observed for TB in solubilized state, can be described as strongly physically adsorbed TB covering the electrode surface. Moreover, the redox process II (observed at -0.05 V) arises from TB covalently immobilized which may decrease

the electron-donating properties of the nitrogen and induce a shift of the redox potential toward more positive values (Schlereth and Schmidt 1995). The voltammogram shown in Fig. 1B was recorded after cycling the modified electrode over the same voltage range in supporting electrolyte (see Fig. S1, SI) to promote desorption of the physically adsorbed TB (Ju et al. 2002; Schlereth and Schmidt 1995) at the electrode surface.

Fig. 1

DPV and EIS techniques, performed in the presence of $[Fe(CN)_6]^{3-/4-}$ redox couple, could give information about the permeability of the redox couple during the preparation process of the TB tailed SAM at the electrode surface. Data obtained (see Figs. S2 and S3, SI, for DPV and EIS data, respectively) confirmed the successful formation of the TB terminated monolayer at the AuSPE surface. After electropolymerization of TB, the disappearance of the redox peaks (see Fig. 3B, curve 1, NIP electrode) indicated that the polymer blocked direct access to the electrode of the redox probe, which made the layer pin-free.

3.3. Preparation of the MIP receptor film

The formation of specific imprints in polymers at the electrode surface was based upon template-functional monomer complexes formed in solution that were preserved until electropolymerization occurred and protein molecules were physically entrapped within the polymer matrix, leading to the formation of specific recognition sites (see Scheme 1).

TB is a small redox-active phenazine derivative carrying a positive charge which have methyl and amine groups attached to the benzene rings and one N substituted by S in the azine ring (see Scheme S1, SI). In aqueous environment, electrostatic interactions, between the cationic dye and the

carboxylate and/or sulphonate groups (ionized at physiologic pH (MacIntosh 1941)) of carbohydrates composing the protein, and multiple H-bonds, between N-H/S-H groups of TB and the O-H/N-H groups present at the *O*-linked glycan moiety on the CA 15-3 antigen (Park et al. 2013), are likely responsible for the formation of the protein-monomer complex.

The surface characteristics, such as the film thickness, concentration of monomer/template used, etc., were carefully optimized in order to increase the analytical performance of the MIP biosensor for CA 15-3 determination in both buffer and serum. For effective *in situ* surface imprinting, the thickness of deposited imprinted film should match the geometric size of anchored biological template (Erdőssy et al. 2016; Wu et al. 2015a). Due to the high molecular weight (≈ 400 kDa) and large dimensions of CA 15-3 (cell-associated mucins were reported to range between 100-500 nm in length and 3–10 nm in diameter (Lai et al. 2009)), the conductive polymer was grown in thickness until maximum electrocatalytic activity was achieved, providing multiple interactions towards CA 15-3 and trap the templates within matrix tightly (maximum spatial confinement of the protein), without compromising both protein template extraction and site accessibility during rebinding stage.

From the experimental point of view, the thickness of polymer film was adjusted by controlling the number of cycles and the scan rate and during cyclic voltammetric electropolymerization. The number of scans performed during the electropolymerization was varied from 10 to 100 and no apparent increase of electroactivity was observed for polymer films that were formed using more than 60 cycles (CV remained constant after 60 continuous sweeps). The effect of the scan rate during electropolymerization was also investigated. Generally, excessively small scan rates result in tight films entrapping the template, while too large scan rates lead to a loose polymer network with low recognition ability (Erdőssy et al. 2016). Thus, electropolymerization of poly(TB) was carried out at a sweep rate of 20 mV s^{-1} (for 60 cycles), improving polymer deposition at the electrode surface and giving origin to a 3D network containing effective imprinted sites for the protein. Additionally, the optimal monomer concentration in the growing-solution was established at 0.5 mmol L^{-1}, according

to our preliminary studies. The concentration of template protein added to the monomer growing solution was 6.7 kU mL^{-1} which was high enough for the grafted MIP layer to readsorb the template protein even at high concentration levels tested, such as 1000 U mL^{-1}.

The CVs of the polymerization process of poly(TB), shown in Fig. 2, were performed between -0.50 and 0.70 V. The irreversible oxidation of the monomer that occurs near the positive end of the potential window produces radical cations that intercouple to give dimers and/or oligomers. In solution, these oligomers are eventually near the TB molecules immobilized at the end of the pre-formed SAM, leading to the further growth of the polymer film and subsequent formation of a 3D network. Data recorded during the electropolymerization process showed the inhibition of poly(TB) deposition at the AuSPE surface in the presence of CA 15-3 (Fig. 2A), when compared with the electropolymerization in absence of template molecule (Fig. 2B). With continuous cycling, the redox peak current at -0.10 V increased gradually at the NIP surface while it remained almost unchanged at the MIP surface. This was attributed to the additional barrier caused by the entrapment within the polymeric matrix of the non-conductive protein.

CVs recorded after the electropolymerization of TB in 0.1 mol L^{-1} PBS (at pH 7.4) containing 0.1 mol L^{-1} $NaNO_3$ are shown in the insets of Figs. 2A and 2B for MIP and NIP surfaces, respectively. The voltammograms were collected after continuous CV cycles in supporting electrolyte solution until stable voltammograms were observed (see Fig. S1, SI) in order to wash-out TB molecules from the modified electrodes and inhibit the monomer-type redox activity (Ju et al. 2002; Schlereth and Schmidt 1995). CVs recorded exhibit two redox couples (peaks I and II´). The negative redox couple I corresponds probably to physically adsorbed and/or occluded unreacted monomer, strongly associated with the polymer matrix, while peak II´, located at more positive potentials, only appears in case of polymer formation and was attributed to redox reaction of the nitrogen bridges between monomer units composing the polymeric matrix (Karyakin et al. 1999; Pauliukaite et al. 2010; Schlereth and Karyakin 1995). As can be seen, polymer formation occurred to a greater extent in NIP

surface than in the MIP surface (peak II´ of NIP >> peak II´ of MIP), which suggested that the protein entrapped inhibits polymer growth and decreases the conductivity of the resulting polymeric film.

Fig. 2

The blocking effect to the redox probe $[Fe(CN)_6]^{3-/4-}$ may be used to investigate the structural differences between the polymerized films in the presence or absence of the template protein. Both, MIP (Fig. 3A, curve 1) and NIP (Fig. 3B, curve 1) modified surfaces, present a high electrochemical blocking effect to the redox process of the redox probe, confirmed by the low peak currents observed when comparing to the voltammogram obtained at the bare AuSPE. This could be explained by the successful entrapment of the protein within the polymeric matrix during electropolymerization and due to the efficient growth of the conducting polymer at the electrode surfaces, giving rise to a thick and very well organized film. The MIP film blocking is more effective than the NIP, because it combined both previous effects.

The washing conditions used for template removal were carefully selected and optimized in order to preserve the integrity of the polymeric network and imprinted sites, while removing as much template as possible (Karimian et al. 2014). Otherwise, the application of the protein MIP receptor in quantitative analysis could be compromised. In this work, CA 15-3 was effectively extracted from the MIP polymeric matrix after continuous potential cycling the electrode surface between 0.00 and 0.40 V, at 50 mV s^{-1}, in 0.1 mol L^{-1} NaOH during 200 cycles (see Fig. S4, SI), followed by subsequent washing with pure water. The voltammetric measurements in the presence of ferro/ferricyanide redox probe performed at the MIP surfaced showed a significant increase of the peak current after template removal from the imprinted surface (Fig. 3A, curve 2) while the voltammograms obtained at the analogous NIP surface (Fig. 3B, curve 2) revealed only a slight

decrease of voltammetric peak current of the redox probe after surface treatment with the extraction solution. Data obtained by EIS in the presence of the ferro/ferricyanide redox probe (Figs. 3C and 3D) also supported the physical entrapment of the protein within the electrogenerated conducting polymeric matrix followed by effective template wash out from MIP surface. The R_{ct} decreased from 7.1 kΩ to 1.1 kΩ (i.e. decreased 85%) after extraction of CA 15-3 from the MIP surface (Fig. 3C) while R_{ct} values remained high (> ≈7 kΩ) before and after treating the NIP surface with the extraction procedure (Fig. 3D), confirming that no severe damage in the polymer network was induced by the washing procedure used.

Fig. 3

Raman measurements were performed to confirm the modification of the Au surface with the TB tailed monolayer and electropolymerized layers of poly(TB) in absence (NIP) and presence (MIP) of template protein (see Fig. S5A-C for basis spectra and Table S1 for their Raman bands, SI). The obtained NIP spectra is very close to the obtained for the thin TB tailed monolayer while the MIP film give rise to a wide range of Raman absorption bands due to the presence of CA 15-3 inside of the polymer film (see Table S1, SI). After protein extraction, the collected Raman spectra for the MIP film was very similar to the obtained for the NIP material, confirming the effective template removal from the imprinted polymer matrix and the chemical similarities between these.

3.4. Analytical performance of the MIP sensor

In order to study the rebinding properties of the prepared CA 15-3 imprinted polymer, the target protein was incubated on the MIP surface for 30 min with the binding buffer (0.1 mol L^{-1} PBS at pH 7.4) containing increasing concentrations of CA 15-3, followed by washing. DPV technique was

selected to monitor the ferro/ferricyanide probe response upon CA 15-3 binding to the receptor surface because it provides a better peak resolution comparing to CV and it is usually more sensitive to smaller changes in the concentrations of target analyte.

Fig. 4A represents the decrease of redox peak currents of the ferro/ferricyanide couple with increasing CA 15-3 concentration from 0.10 U mL^{-1} to 1000 U mL^{-1}. Successful rebinding of the template protein was observed. The investigation of the binding performance was also made using NIP electrode (Fig. 4B). The polymer film deposited on the electrode in the absence of protein, but treated the same way as that of MIP, shows a very narrow response to the protein biomarker.

In Fig. 4C, the peak current obtained by DPV was plotted as a function of the logarithm of CA 15-3 concentration (in U mL^{-1}). Good linearity was achieved (R^2 = 0.987) over the concentration range from 0.10 to 100 U mL^{-1}. The sensitivity obtained with the MIP sensor is about ~9 times superior to the sensitivity obtained with NIP sensor, suggesting that the recognition of CA 15-3 on the MIP surface was made through the imprinted sites and the contribution of non-specific response was negligible. After the investigation of the NIP sensor response, only a slight decrease of the redox peak current was obtained even for high concentration levels of CA 15-3, revealing a poor contribution of non-specific binding to the electrochemical signal.

The LOD obtained by the MIP sensor was estimated according to Recommendations of IUPAC for ion-selective electrodes (Buck and Lindner 1994). The LOD obtained was of the same order of magnitude than other LODs reported in literature using both, non-electrochemical and electrochemical, immunosensor devices (see Table S2, SI). Also comparing to other methods, this work yielded the best lower limit of linear range, allowing the quantification of CA 15-3 down to 0.10 U mL^{-1}, well below the threshold needed for clinical evaluating progression and recurrence of breast carcinoma (cut-off value of 30 U mL^{-1} (Chourin et al. 2009; Duffy et al. 2004; Sölétormos et al. 2004)). It also has a wide concentration range of response, allowing a direct analysis of samples above the cut-off value.

Binding affinity in the MIP system was evaluated by adjusting the experimental data to the Freundlich isotherm:

$$I_0 - I = K_F . C_e^{\,1/n_F} \quad (1)$$

where K_F is the Freundlich constant, n_F the Freundlich exponent, (I_0-I) is the adsorbed amount at equilibrium and C_e (U mL^{-1}) the equilibrium concentration. The fit of the binding isotherm to the MIP and NIP synthetic receptor films is shown in Fig. 4D. An impressive ~12-fold increase in the binding affinity of CA 15-3 to MIP (K_F = 7.1 (± 0.3) × 10^{-6} A $mL^{1/n}$ $U^{-1/n}$) when compared to NIP (K_F = 6.0 (± 0.4) × 10^{-7} A $mL^{1/n}$ $U^{-1/n}$) receptor was obtained, demonstrating the effectiveness of this approach in creating an efficient synthetic receptor for the target protein. The n_F values obtained for MIP and NIP systems, of 6.4 ± 0.3 and 7.0 ± 0.6, respectively, indicates that for low concentration levels the amount of bound protein greatly increased with small changes in C_e, while at larger concentrations of protein the adsorption intensity weakened (more imprinted sites were rebound) and saturation occurred (analytical signal remained constant).

Fig. 4

3.5. Analytical application feasibility

CA 15-3 detection in the presence of potential biological interfering components was carried out to investigate the usability of the fabricated MIP sensor. Diluted artificial serum (1:10, in 0.1 mol L^{-1} PBS pH 7.4) was used for this purpose. Ferro/ferricyanide probe redox signal was monitored by DPV upon binding of CA 15-3 to the imprinted surface.

The voltammograms collected for the different CA 15-3 concentrations prepared in diluted artificial serum and the corresponding plot representing the correlation between the peak current and the concentration of CA 15-3 are shown in Fig. 5. The sensitivity of the CA 15-3 MIP biosensor in the diluted artificial serum (-3.12×10^{-6} A/decade $C_{CA\ 15\text{-}3}$, U mL^{-1}) was very similar to that obtained in PBS (-2.98×10^{-6} A/decade $C_{CA\ 15\text{-}3}$, U mL^{-1}; increase of +4.5%) allowing to conclude that serum matrix had no significant contribution to the analytical signal. It also suggested that the observed decrease of redox probe response was only due to the specific binding of CA 15-3 in diluted serum to the MIP receptor film. The sensor detection limit was <0.10 U mL^{-1}. This high sensitivity enables the determination of low concentrations of CA 15-3 in diluted serum as the normal serum level of CA 15- 3 is usually less than 30 U mL^{-1}.

Fig. 5

Recovery studies performed with MIP biosensor were conducted in diluted serum samples spiked with known amounts of CA 15-3. The concentration found was calculated from the standard calibration curve after repeated measurements performed on the samples tested (see Table S3, SI). The concentration values found were in good agreement with spiked ones, having high detection recoveries (between 99 and 102%). Also, the errors affecting the concentration found were considered to be acceptable (RSD values for n=3 were less than 11%). These results further corfirmed the high analytical performance of the as-fabricated MIP biosensor, enabling CA 15-3 detection with high selectivity and sensitivity in artifitial serum samples.

4. Conclusions

In this work, a particular advantage arises from surface modification with electronically conducting polymer poly(TB), which greatly improved the sensing performance of the fabricated MIP sensor towards breast cancer biomarker CA 15-3. Strategically, the electrosynthesized MIP receptor film was connected to a TB terminated SAM tethered to the Au surface through Au–S bonds which caused uniform and efficient nucleation-and-growth of the polymer film and greatly enhanced the stability against degradation of the MIP film at the electrode surface.

The desired imprinting effect was achieved after optimization of the film thickness during electropolymerization to match the template size, giving origin to well-defined binding sites after successful template extraction. Moreover, rebinding affinity studies, performed by fitting Freundlich isotherm to experimental data, indicated the existence of effective imprinting cavities in such MIP film with excellent affinity for the imprinted protein (~12-fold when compared to NIP, based K_F values).

The selective adsorption of CA 15-3 onto MIP film (after 30 min incubation) induced a significant reduction of redox probe currents. Calibration plots obtained showed a linear dependency of peak current over a wide CA 15-3 concentration range (from 0.10 U mL^{-1} to 100 U mL^{-1}). LODs obtained (< 0.10 U mL^{-1}) in buffer and in artificial serum showed that the MIP biosensor was capable of detecting CA 15-3 at clinically relevant concentration levels (cut of values).

In general, the developed device provides a new strategy for label-free, rapid, simple and cost-effective screening of CA 15-3 biomarker. Furthermore, the inherent characteristics of the rigid polymer used may lead to robustness, long-term storage stability and potential re-usability of the prepared MIP biosensor. The overall approach seems suitable for point-of-care use in clinical context.

Acknowledgments

This research had the financial support of FP7/European Research Council through the Starting Grant 3P's (ERC/Stg/GA311086) given to MGFS and FCT (Fundação para a Ciência e Tecnologia) and co-financed by the European Union (FEDER funds) under the Partnership Agreement PT2020, through project POCI/01/0145/FEDER/006980 with reference UID/QUI/UI0081/2013 (CIQUP), by NORTE-2020 and COMPETE 2020 through projects NORTE-01-0145-FEDER-000029 and NORTE-01-0247-FEDER-017834. JAR (ref. SFRH/BPD/105395/2014) acknowledges FCT under the QREN – POPH – Advanced Training, subsidized by European Union and national MEC funds.

Refereces

Akter, R., Jeong, B., Choi, J.-S., Rahman, M.A., 2016. Biosens. Bioelectron. 80, 123-130.

Ambrosi, A., Airò, F., Merkoçi, A., 2010. Anal. Chem. 82, 1151-1156.

Arias, F., Godínez, L.A., Wilson, S.R., Kaifer, A.E., Echegoyen, L., 1996. J. Am. Chem. Soc. 118, 6086-6087.

Balint, R., Cassidy, N.J., Cartmell, S.H., 2014. Acta Biomater. 10, 2341-2353.

Buck, R.P., Lindner, E., 1994. Pure Appl. Chem. 66, 2527-2536.

Cai, C.-X., Xue, K.-H., 1998. Talanta 47, 1107-1119.

Chang, C.-C., Chiu, N.-F., Lin, D.S., Chu-Su, Y., Liang, Y.-H., Lin, C.-W., 2010. Anal. Chem. 82, 1207-1212.

Chang, H., Wang, X., Shiu, K.-K., Zhu, Y., Wang, J., Li, Q., Chen, B., Jiang, H., 2013. Biosens. Bioelectron. 41, 789-794.

Chourin, S., Georgescu, D., Gray, C., Guillemet, C., Loeb, A., Veyret, C., Basuyau, J.P., 2009. Ann. Oncol. 20, 962-964.

Darwish, I.A., Wani, T.A., Khalil, N.Y., Blake, D.A., 2012. Talanta 97, 499-504.

Duffy, M.J., Duggan, C., Keane, R., Hill, A.D.K., McDermott, E., Crown, J., O'Higgins, N., 2004. Clin. Chem. 50, 559-563.

Erdőssy, J., Horváth, V., Yarman, A., Scheller, F.W., Gyurcsányi, R.E., 2016. Trends Anal. Chem. 79, 179-190.

Fragoso, A., Latta, D., Laboria, N., von Germar, F., Hansen-Hagge, T.E., Kemmner, W., Gartner, C., Klemm, R., Drese, K.S., O'Sullivan, C.K., 2011. Lab Chip 11, 625-631.

Fu, Z., Yang, Z., Tang, J., Liu, H., Yan, F., Ju, H., 2007. Anal. Chem. 79, 7376-7382.

Ge, S., Jiao, X., Chen, D., 2012a. Analyst 137(19), 4440-4447.

Ge, S., Yu, F., Ge, L., Yan, M., Yu, J., Chen, D., 2012b. Analyst 137, 4727-4733.

Gonzalez, R.M., Seurynck-Servoss, S.L., Crowley, S.A., Brown, M., Omenn, G.S., Hayes, D.F., Zangar, R.C., 2008. J. Proteome Res. 7, 2406-2414.

Gui, R., Jin, H., Guo, H., Wang, Z., 2018. Biosens. Bioelectron. 100, 56-70.

Jemal, A., Center, M.M., DeSantis, C., Ward, E.M., 2010. Cancer Epidemiol. Biomarkers Prev. 19, 1893-1907.

Jiang, D., Tang, J., Liu, B., Yang, P., Shen, X., Kong, J., 2003. Biosens. Bioelectron. 18, 1183-1191.

Jiang, X., Wang, H., Yuan, R., Chai, Y., 2015. Biosens. Bioelectron. 63, 33-38.

Jin, H., Gui, R., Gong, J., Huang, W., 2017. Biosens Bioelectron. 92, 378-384.

Ju, H., Xiao, Y., Lu, X., Chen, H., 2002. J. Electroanal. Chem. 518, 123-130.

Karimian, N., Turner, A.P.F., Tiwari, A., 2014. Biosens. Bioelectron. 59, 160-165.

Karyakin, A.A., Karyakina, E.E., Schmidt, H.-L., 1999. Electroanalysis 11, 149-155.

Kryscio, D.R., Peppas, N.A., 2012. Acta Biomater. 8, 461-473.

Lai, S.K., Wang, Y.-Y., Hanes, J., 2009. Adv. Drug Deliv. Rev. 61, 158-171.

Li, H., He, J., Li, S., Turner, A.P.F., 2013. Biosens. Bioelectron. 43, 25-29.

Li, M., Kang, J.W., Sukumar, S., Dasari, R.R., Barman, I., 2015. Chem. Sci. 6, 3906-3914.

Li, W., Yuan, R., Chai, Y., Chen, S., 2010. Biosens. Bioelectron. 25, 2548-2552.

Liu, B., Li, Q., Zhang, B., Cui, Y., Chen, H., Chen, G., Tang, D., 2011. Nanoscale 3, 2220-2226.

Lu, L.-M., Wang, S.-P., Qu, F.-L., Zhang, X.-B., Huan, S., Shen, G.-L., Yu, R.-Q., 2009. Electroanalysis 21, 1152-1158.

MacIntosh, F.C., 1941. Biochem. J. 35, 776-782.

Malitesta, C., Mazzotta, E., Picca, R.A., Poma, A., Chianella, I., Piletsky, S.A., 2012. Anal. Bioanal. Chem. 402, 1827-1846.

Mažeikienė, R., Niaura, G., Malinauskas, A., 2008. Electrochim. Acta 53, 7736-7743.

Moon, J.-M., Kim, D.-M., Kim, M.H., Han, J.-Y., Jung, D.-K., Shim, Y.-B., 2017. Biosens. Bioelectron. 91, 128-135.

Moreira, F.T.C., Sharma, S., Dutra, R.A.F., Noronha, J.P.C., Cass, A.E.G., Sales, M.G.F., 2014. Sens. Actuators B Chem. 196, 123-132.

Park, Y.M., Kim, S.J., Kim, K., Han, Y.D., Yang, S.S., Yoon, H.C., 2013. Sens. Actuators B Chem. 186, 571-579.

Pauliukaite, R., Ghica, M.E., Barsan, M.M., Brett, C.M.A., 2010. Anal. Lett. 43, 1588-1608.

Peng, H.-P., Hu, Y., Liu, P., Deng, Y.-N., Wang, P., Chen, W., Liu, A.-L., Chen, Y.-Z., Lin, X.-H., 2015. Sens. Actuators B Chem. 207, 269-276.

Pud, A.A., 1994. Synth. Met. 66, 1-18.

Rebelo, T.S.C.R., Santos, C., Costa-Rodrigues, J., Fernandes, M.H., Noronha, J.P., Sales, M.G.F., 2014. Electrochim. Acta 132, 142-150.

Ribeiro, J.A., Pereira, C.M., Silva, A.F., Sales, M.G.F., 2017. Anal. Chim. Acta 981, 41-52.

Sayıklı Şimşek, Ç., Nur Sonuç Karaboğa, M., Sezgintürk, M.K., 2015. Talanta 144, 210-218.

Schlereth, D.D., Karyakin, A.A., 1995. J. Electroanal. Chem. 395, 221-232.

Schlereth, D.D., Schmidt, H.-L., 1995. J. Electroanal. Chem. 380, 117-125.

Sharma, P.S., Pietrzyk-Le, A., D'Souza, F., Kutner, W., 2012. Anal. Bioanal. Chem. 402, 3177-3204.

Sturgeon, C.M., Duffy, M.J., Stenman, U.-H., Lilja, H., Brünner, N., Chan, D.W., Babaian, R., Bast, R.C., Dowell, B., Esteva, F.J., Haglund, C., Harbeck, N., Hayes, D.F., Holten-Andersen, M., Klee, G.G., Lamerz, R., Looijenga, L.H., Molina, R., Nielsen, H.J., Rittenhouse, H., Semjonow, A., Shih, I.-M., Sibley, P., Sölétormos, G., Stephan, C., Sokoll, L., Hoffman, B.R., Diamandis, E.P., 2008. Clin. Chem. 54, e11-e79.

Sölétormos, G., Nielsen, D., Schiøler, V., Mouridsen, H., Dombernowsky, P., 2004. Eur. J. Cancer 40, 481-486.

Thenmozhi, K., Narayanan, S.S., 2017. Mater. Sci. Eng. C 70, 223-230.

Wang, G., Qing, Y., Shan, J., Jin, F., Yuan, R., Wang, D., 2013. Microchim. Acta 180, 651-657.

Wang, W., Wang, F., Yao, Y., Hu, S., Shiu, K.-K., 2010. Electrochim. Acta 55, 7055-7060.

Wang, Y., Hu, S., 2006. Biosens. Bioelectron. 22, 10-17.

Wang, Y., Li, X., Cao, W., Li, Y., Li, H., Du, B., Wei, Q., 2014a. Talanta 129, 411-416.

Wang, Y., Li, X., Cao, W., Li, Y., Li, H., Du, B., Wei, Q., 2014b. Biosens. Bioelectron. 61, 618-624.

Whitcombe, M.J., Chianella, I., Larcombe, L., Piletsky, S.A., Noble, J., Porter, R., Horgan, A., 2011. Chem. Soc. Rev. 40, 1547-1571.

Willner, I., Doron, A., Katz, E., Levi, S., Frank, A.J., 1996. Langmuir 12, 946-954.

Willner, I., Riklin, A., 1994. Anal. Chem. 66, 1535-1539.

Wu, G., Li, J., Qu, X., Zhang, Y., Hong, H., Liu, C., 2015a. RSC Adv. 5, 47010-47021.

Wu, K., Zhang, Y., Wang, Y., Ge, S., Yan, M., Yu, J., Song, X., 2015b. ACS Appl. Mater. Interfaces 7, 24330-24337.

Xiao, Y., Ju, H.-X., Chen, H.-Y., 1999. Anal. Chim. Acta 391, 73-82.

Ye, L., Mosbach, K., 2008. Chem. Mater. 20, 859-868.

Zhai, X., Li, Y., Liu, G., Cao, Y., Gao, H., Yue, C., Sheng, N., 2013. Sens. Actuators B Chem. 178, 169-175.

Zhang, M., Gorski, W., 2005. J. Am. Chem. Soc. 127, 2058-2059.

Zhang, X., Peng, X., Jin, W., 2006. Anal. Chim. Acta 558, 110-114.

Zhu, H., Dale, P.S., Caldwell, C.W., Fan, X., 2009. Anal. Chem. 81, 9858-9865.

Zong, C., Wu, J., Wang, C., Ju, H., Yan, F., 2012. Anal. Chem. 84, 2410-2415.

List of Figures and Schemes

Scheme 1. Schematic representation of molecular imprinting and the recognition principle of the MIP sensor for CA 15-3 detection. First, the formation of the (A) Toluidine blue terminated monolayer was achieved via (1) glutaraldehyde on a preformed AOT SAM on AuSPEs, followed by (2) immobilization of TB molecules. Then, (B) template and functional monomer interacted to form the binding sites preserved by electropolymerization of TB. The subsequent (C) template removal leaves rebinding empty cavities. Electrochemical (CV, SWV and EIS in the presence of $[Fe(CN)_6]^{3-/4-}$ redox probe) and Raman spectroscopy studies of MIP electrode were performed at this point. In the last step, the (D) template rebinding to the binding sites allows the electrochemical detection of the protein by the prepared MIP electrode, using DPV (in the presence of $[Fe(CN)_6]^{3-/4-}$ redox probe).

Fig. 1. (A) CVs of the preparation process of the TB terminated monolayer in 0.1 mol L^{-1} PBS (at pH 7.4) containing 0.5 mmol L^{-1} TB for 10 cycles. Scan rate: 50 mV s^{-1}. (B) CV of the TB monolayer in 0.1 mol L^{-1} PBS (at pH 7.4). Scan rate: 50 mV s^{-1}. Inset: DPV obtained in the same experimental conditions.

Fig. 2. (A) MIP and (B) NIP surface preparation by CV electropolymerization of 0.5 mmol L^{-1} TB in 0.1 mol L^{-1} PBS (at pH 7.4) in absence (NIP, B) and presence (MIP, A) of 6.7 kU mL^{-1} CA 15-3. Scan rate: 20 mV s^{-1}; Number of scans: 60. Insets: CVs recorded with the prepared MIP and NIP surfaces in 0.1 mol L^{-1} PBS (at pH 7.4). Scan rate: 50 mV s^{-1}.

Fig. 3. (A, B) CVs and (C, D) complex impedance plots obtained in presence of 5 mmol L^{-1} $[Fe(CN)_6]^{3-/4-}$ redox probe with MIP (A, C) and NIP (B, D) modified AuSPEs before (curves 1) and after (curves 2) extraction of template protein by consecutive CV cycles in 0.1 mol L^{-1} NaOH. For comparison, the voltammogram obtained with bare gold electrode was included in CV data. Scan rate: 50 mV s^{-1}. Insets: DPVs obtained at the same experimental condition.

Fig. 4. Electrochemical DPV evaluation in presence of 5 mmol L^{-1} $[Fe(CN)_6]^{3-/4-}$ redox probe of template rebinding with (A) MIP and (B) NIP receptor films, after incubation in different concentrations of CA 15-3 (from 0.10 U mL^{-1} to 1000 U mL^{-1}, in 0.1 mol L^{-1} PBS pH 7.4) for 30 min. (C) The plots of peak current *versus* the logarithmic concentration of CA 15- 3 on MIP and NIP receptor films. Inset: Relationship between the peak current and the concentration of CA 15-3 for MIP and NIP receptors. (D) Binding isotherm of synthetic MIP and NIP receptor films at different concentrations of CA 15-3. Dotted lines represents the fitting of Freundlich isotherm to the experimental data.

Fig. 5: (A) DPVs obtained in presence of 5 mmol L^{-1} $[Fe(CN)_6]^{3-/4-}$ redox probe with MIP receptor film after incubation in different concentrations of CA 15-3 (from 0.1 U mL^{-1} to 1000 U mL^{-1}, in diluted artificial serum) for 30 min. (B) Relationship between the peak current and the concentration of CA 15-3 in diluted artificial serum. Inset: The plot of peak current *versus* CA 15-3 concentration in logarithmic coordinates.

Scheme 1

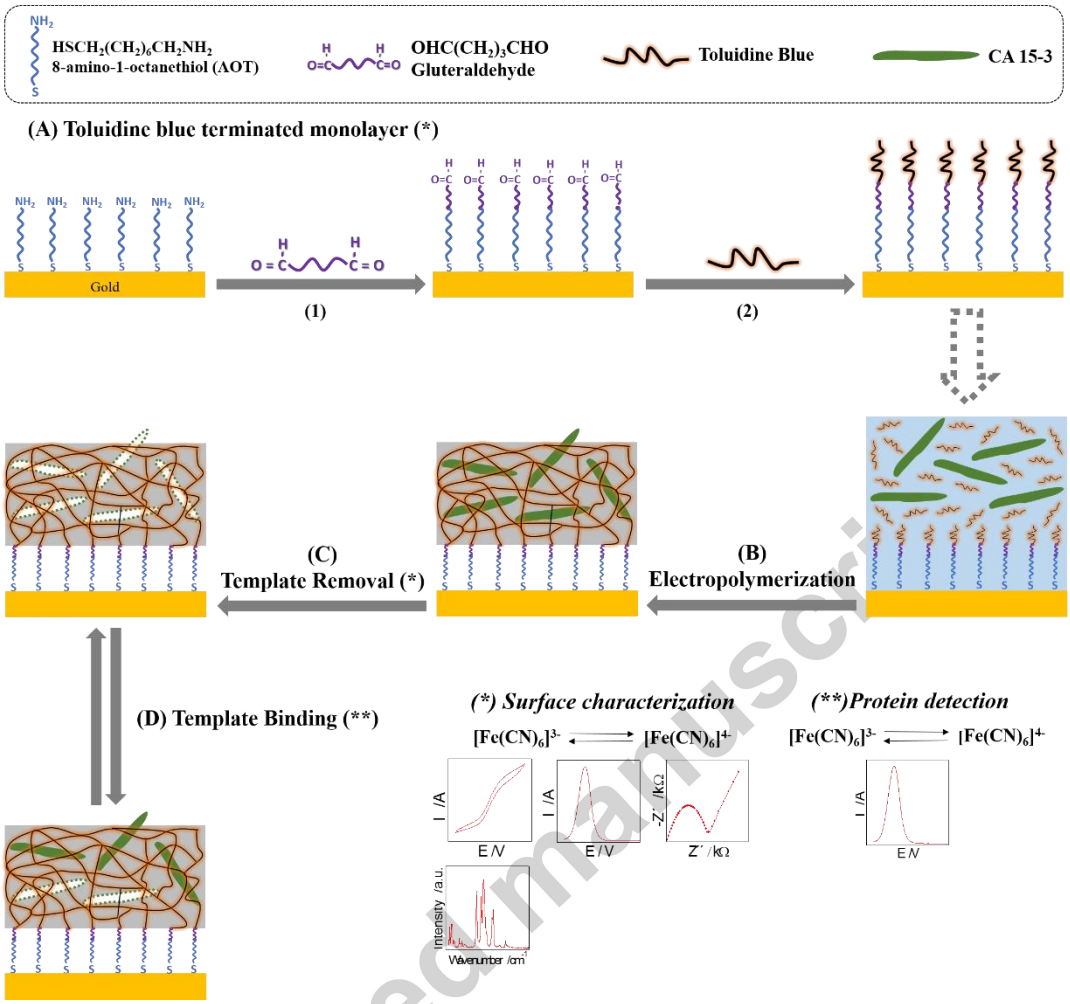

Fig. 1

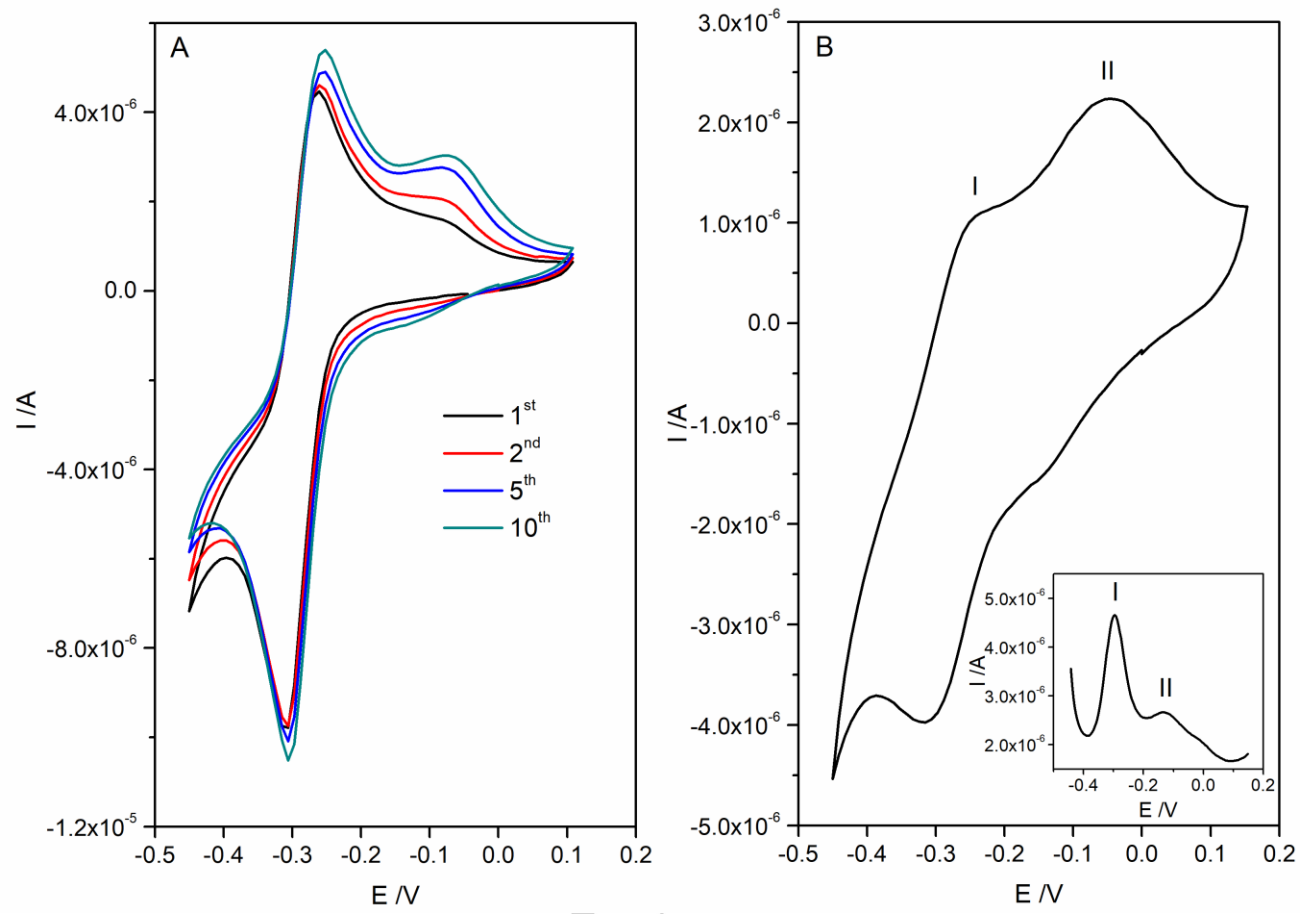

Fig. 2

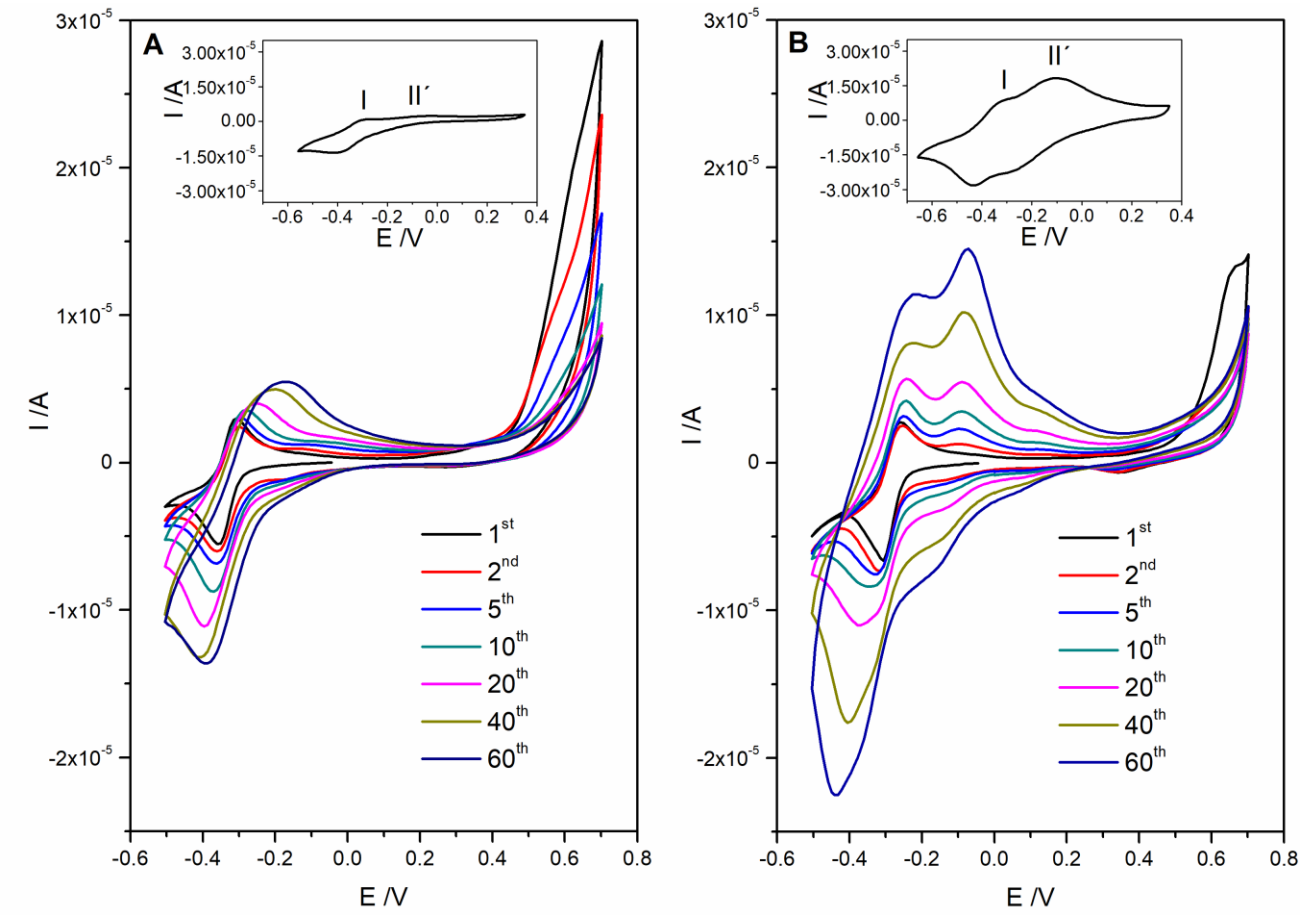

Fig. 3

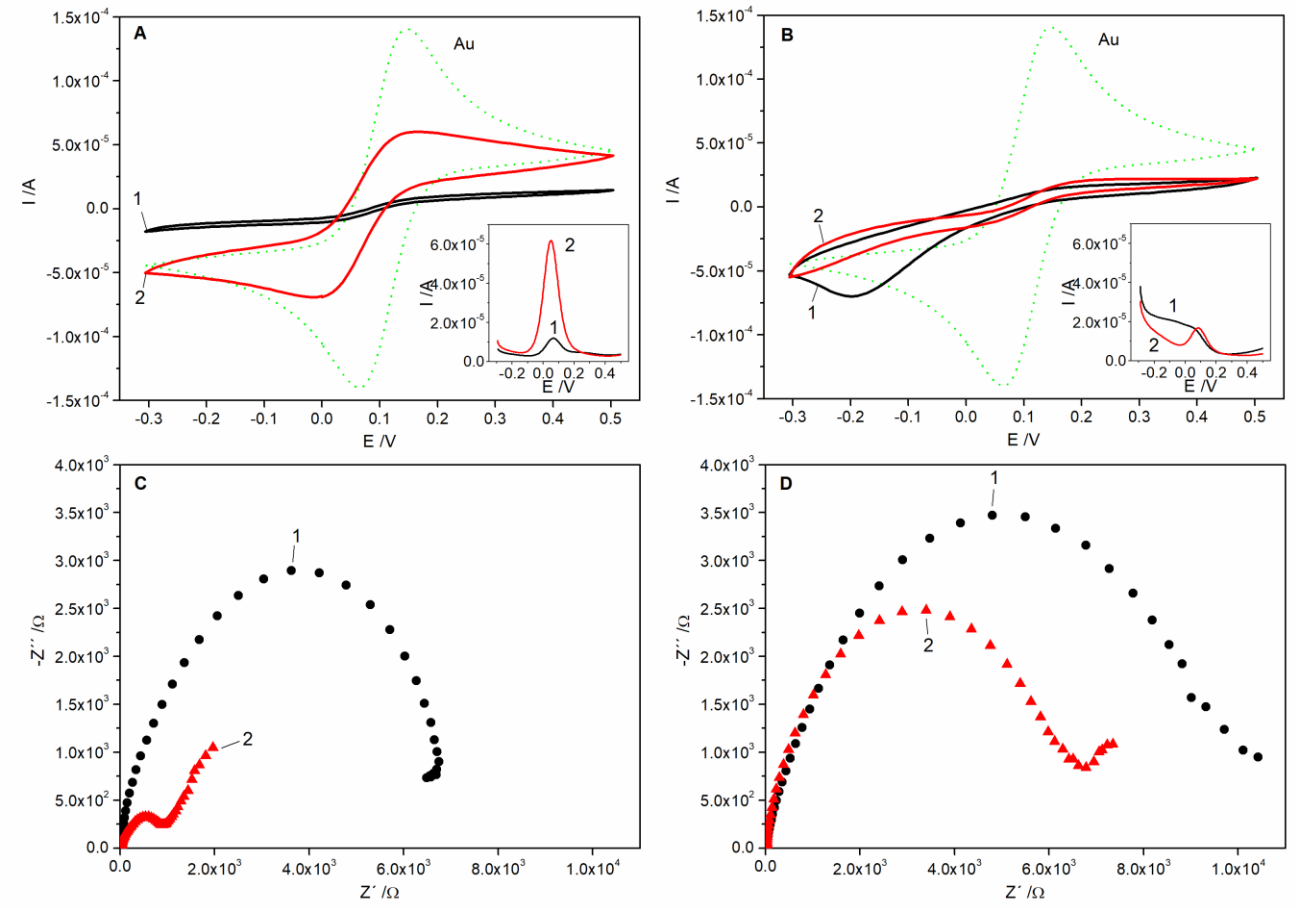

Fig. 4 (new data included in Figs. 4A and C)

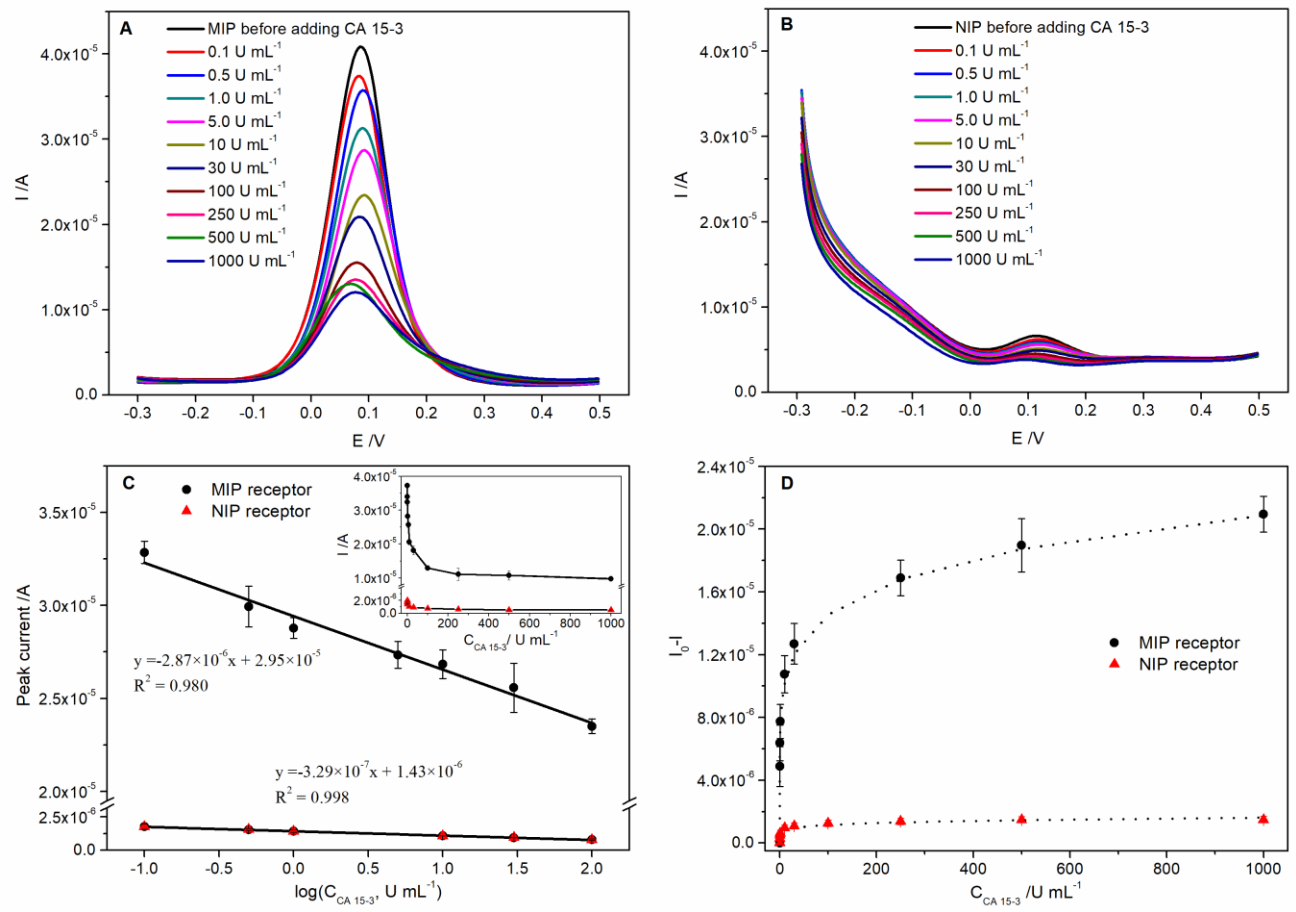

Fig. 5

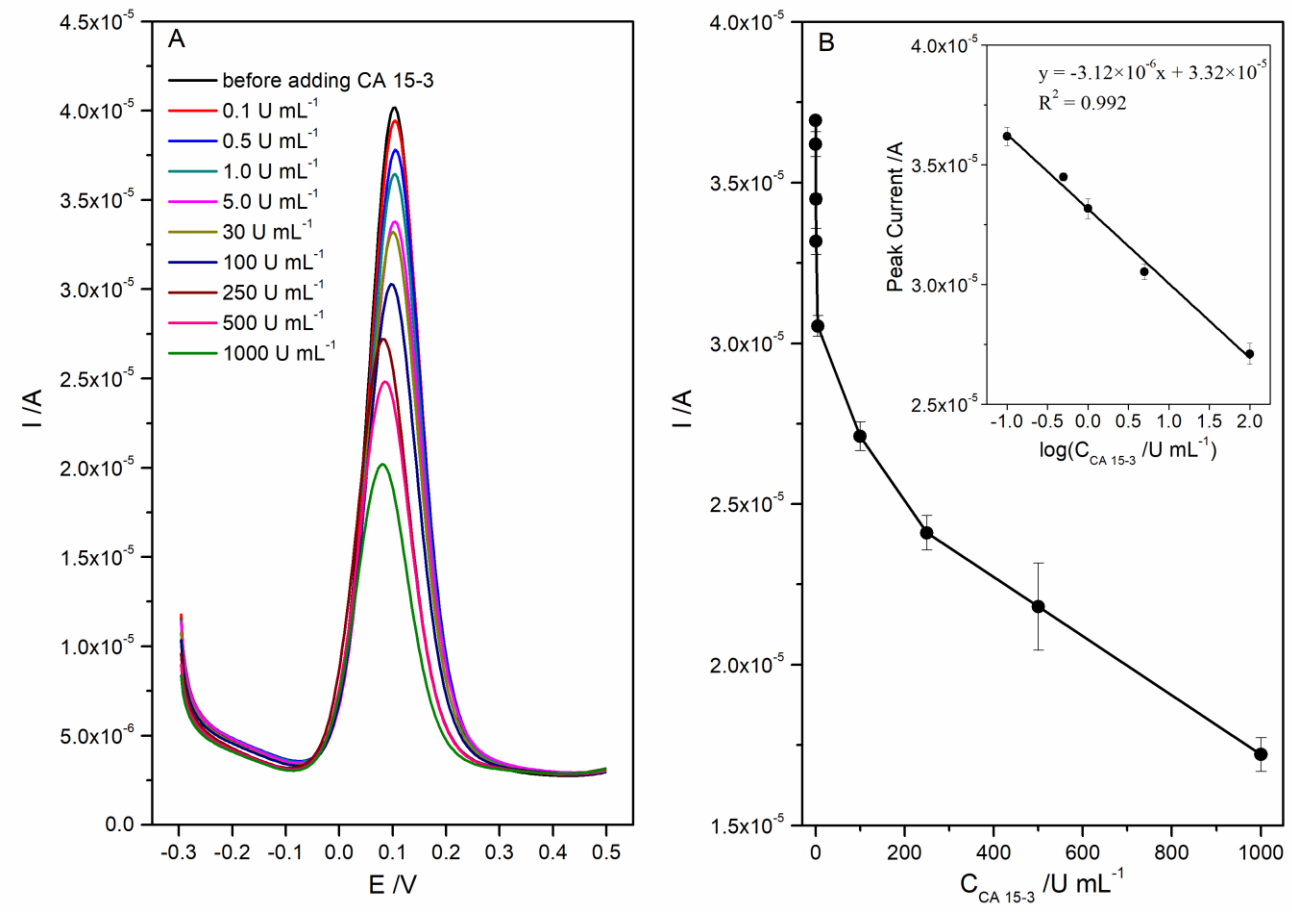

Highlights

- Electrochemical biosensor for detection of breast cancer biomarker CA 15-3;
- MIPs and SPEs were combined for the simple and fast screening of CA 15-3 in PoC;
- Synthetic receptor prepared by electropolymerization of Toluidine Blue on Au electrode;
- Determination of serum CA 15-3 at clinically relevant levels (LOD < 0.1 U mL^{-1}).